

Ferroelectric order in liquid crystal phases of polar disk-shaped ellipsoids

Tushar Kanti Bose* and Jayashree Saha†

Department of Physics, University of Calcutta, 92 Acharya Prafulla Chandra Road, Kolkata-700009, India

(Received 21 February 2014; published 23 May 2014)

The demonstration of a spontaneous macroscopic ferroelectric order in liquid phases in the absence of any long range positional order is considered an outstanding problem of both fundamental and technological interest. Recently, we reported that a system of polar achiral disklike ellipsoids can spontaneously exhibit a long searched ferroelectric nematic phase and a ferroelectric columnar phase with strong axial polarization. The major role is played by the dipolar interactions. The model system of interest consists of attractive-repulsive Gay-Berne oblate ellipsoids embedded with two parallel point dipoles positioned symmetrically on the equatorial plane of the ellipsoids. In the present work, we investigate in detail the profound effects of changing the separation between the two symmetrically placed dipoles and the strength of the dipoles upon the existence of different ferroelectric discotic liquid crystal phases via extensive off-lattice N - P - T Monte Carlo simulations. Ferroelectric biaxial phases are exhibited in addition to the uniaxial ferroelectric fluids where the phase biaxiality results from the dipolar interactions. The structures of all the ferroelectric configurations of interest are presented in detail. Simple phase diagrams are determined which include different polar and apolar discotic fluids generated by the system.

DOI: [10.1103/PhysRevE.89.052509](https://doi.org/10.1103/PhysRevE.89.052509)

PACS number(s): 64.70.M-, 64.70.pp, 77.80.-e, 82.20.Wt

I. INTRODUCTION

Conventional ferroelectric materials are solid. It is generally difficult to realize spontaneous ferroelectric order in fluid phases. In the absence of external fields, the molecules easily reorient themselves to cancel any global polarization. The development of fluid phases with an overall polarization is a topic which attracts great interest from both fundamental and practical viewpoints [1,2]. The least ordered conceivable ferroelectric phase is the ferroelectric nematic liquid crystal (FNLC) phase, which is characterized by a spontaneous macroscopic polarization, particle mobilities typical of liquids, and the complete absence of any long range positional order. However, practical realization of such a phase is a long standing problem [1,2]. The FNLC phase is expected to exhibit a much faster and easier response to an external field compared to the known ferroelectric smectic liquid crystals, and hence it could open new avenues in electrooptic display technology.

Theoretical studies have shown that there is no fundamental reason to forbid a ferroelectric nematic order [3–9]. A ferroelectric response was recently observed in a nematic phase of bent core molecules under an external field, but ferroelectric order in the absence of the field was not achieved [10]. From computer simulation studies, it has been found that model spherical particles with a strong central dipole moment exhibit a FNLC phase [4,5,11,12]. Ferroelectric order in these systems is developed solely due to the dipolar interactions and the lack of orientational bias of the spherical particles. On the contrary, an overall polarization is very rare in systems of anisotropic molecules which spontaneously form orientationally ordered liquid crystal phases. Computer simulation studies of hard anisotropic ellipsoids, spherocylinders, and cut spheres with permanent dipole moments have not established a global ferroelectric order [5,13–16].

Similar attempts considering ellipsoidal particles interacting via attractive-repulsive Gay-Berne (GB) potential with point dipole moments have also failed to yield a ferroelectric liquid crystal [17–23]. Ayton *et al.* showed that as the length to breadth ratio decreases from unity, the tendency to form a ferroelectric nematic phase gradually decreases for hard discotic ellipsoidal particles with strong central dipoles [24]. Ayton and Patey also found that the FNLC phase can be obtained with a system of discotic hard cut spheres with a uniform distribution of axial dipoles in the central circular patch, but the assumption of uniform dipolar distribution and that of complete orientational order of disks make the system a rather idealized one [25]. Currently, the idea from both theoretical and practical points of view is that a liquid ferroelectric order cannot be discovered easily. It is essential to find appropriate microscopic interactions to design a FNLC phase.

Recently, we found that a system of polar achiral disklike ellipsoids can spontaneously exhibit a long searched FNLC phase [26]. The model system of interest consists of attractive-repulsive Gay-Berne oblate ellipsoids embedded with two parallel point dipoles positioned symmetrically on the equatorial plane of the ellipsoids. At lower temperature, the FNLC phase condenses to a ferroelectric hexagonal columnar fluid with an axial macroscopic polarization. A spontaneous ferroelectric order of dipolar origin was thus demonstrated in the columnar phase of disklike particles; earlier simulation studies of dipolar cut spheres and disk shaped particles only yielded antiferroelectric columnar phases with partial or fully polarized individual columns without any global polarization [5,16,21]. The realization of a ferroelectric columnar (FCoI) phase with an axial macroscopic polarization is also considered an interesting puzzle in soft matter physics and chemistry. Several attempts to develop a ferroelectric columnar phase in different anisotropic molecular systems has been reported in the past 40 years [27].

However, the goal of achieving columnar liquid crystals with axial macroscopic polarization at zero electric field

*tkb.bose@gmail.com

†jsphy@caluniv.ac.in

and its electrical invertibility remained unsolved [28]. Such materials are considered potential candidates for ultrahigh-density memory devices. Recently, ferroelectric behavior was observed in columnar liquid crystals adopting a core-shell architecture [28]. As the system of dipolar Gay-Berne oblate ellipsoids successfully exhibits a FNLC phase and a ferroelectric columnar phase [26], it becomes essentially important to investigate the influences of dipolar interactions upon the existence of different ferroelectric fluids to gain a complete understanding of the structure-property relationship, which might be helpful for future development of the technologically important fluid ferroelectric materials. It is evident that both the separation between two dipoles on the ellipsoids and the dipole strength have significant roles in determining the stability of different ferroelectric liquid crystal phases of dipolar origin.

In the present work, we have systematically explored the phase behavior of the model particles for various dipolar separations and dipole strengths to understand their influence upon the existence of different ferroelectric phases of interest. In Sec. II we detail the molecular model and pair interactions. The simulation methods are described in Sec. III. In Sec. IV we describe the simulation results. Simple phase diagrams based on the results are presented in Sec. V, and Sec. VI concludes the paper.

II. THE MOLECULAR MODEL AND INTERACTIONS

In this paper we present computer simulations of uniaxial oblate ellipsoids of revolution where each ellipsoid is embedded with two axial off-center parallel point dipole moments. The dipoles are symmetrically positioned on the equatorial plane of the ellipsoid, at equal distances from the center of the ellipsoid. The dipoles are placed on the molecular x axis (perpendicular to the symmetry axis) of each GB molecule, separated by a distance $d^* \equiv d/\sigma_0$ along the axis. The dipolar ellipsoids are interacting via a pair potential, which is the sum of a modified form of the GB potential [29] and the electrostatic dipolar interactions. In the modified form for a discotic liquid crystal [30], the pair potential between two oblate ellipsoids i and j is given by

$$U_{ij}^{\text{GB}}(\mathbf{r}_{ij}, \hat{\mathbf{u}}_i, \hat{\mathbf{u}}_j) = 4\epsilon(\hat{\mathbf{r}}_{ij}, \hat{\mathbf{u}}_i, \hat{\mathbf{u}}_j)(\rho_{ij}^{-12} - \rho_{ij}^{-6}),$$

where $\rho_{ij} = [r_{ij} - \sigma(\mathbf{r}_{ij}, \hat{\mathbf{u}}_i, \hat{\mathbf{u}}_j) + \sigma_e]/\sigma_e$. Here unit vectors $\hat{\mathbf{u}}_i$ and $\hat{\mathbf{u}}_j$ represent the orientations of the symmetry axes of the molecules, $\mathbf{r}_{ij} = r_{ij}\hat{\mathbf{r}}_{ij}$ is the separation vector of length r_{ij} between the centers of mass of the ellipsoids, and σ_e is the minimum separation between two ellipsoids in a face-to-face configuration determining the thickness of the ellipsoids. The anisotropic contact distance σ and the depth of the pair interaction well ϵ are dependent on four important parameters κ, κ', μ and ν , as defined in [30]. Here $\kappa = \sigma_e/\sigma_0$ is the aspect ratio of the ellipsoids, where σ_0 is the minimum separation between two ellipsoids in a side-by-side configuration; $\kappa' = \epsilon_s/\epsilon_e$ is the ratio of interaction well depths in side-by-side and face-to-face configurations of the disk shaped ellipsoids. The other two parameters, μ and ν , control the well depth of the potential. σ_0 and ϵ_0 define the length and energy scales, respectively, where ϵ_0 is the well depth in the cross configuration. The values used here to study

the bulk phase behavior are $\kappa = 0.345, \kappa' = 0.2, \mu = 1, \nu = 3$. The value of κ is obtained from the parametrization of the GB potential that mimics the interaction between two molecules of triphenylene [31], which is known to form the core of many discotic mesogens [32]. The other parameters were chosen from previous works on discotic liquid crystals which exhibited discotic nematic and hexagonal columnar phases [21–23].

The electrostatic interaction energy between two such dipolar ellipsoids is given by $U_{ij}^{\text{dd}} = \sum_{\alpha, \beta=1}^2 \frac{\mu^2}{r_{\alpha\beta}^3} [(\hat{\boldsymbol{\mu}}_{i\alpha} \cdot \hat{\boldsymbol{\mu}}_{j\beta}) - 3(\hat{\boldsymbol{\mu}}_{i\alpha} \cdot \hat{\mathbf{r}}_{\alpha\beta})(\hat{\boldsymbol{\mu}}_{j\beta} \cdot \hat{\mathbf{r}}_{\alpha\beta})]$, where $\mathbf{r}_{\alpha\beta} (= \mathbf{r}_{j\beta} - \mathbf{r}_{i\alpha})$ is the vector joining the two point dipoles $\boldsymbol{\mu}_{i\alpha}$ and $\boldsymbol{\mu}_{j\beta}$ on molecules i and j at the positions $\mathbf{r}_{i\alpha} = \mathbf{r}_i \pm \frac{d}{2}\hat{\mathbf{x}}_i$ and $\mathbf{r}_{j\beta} = \mathbf{r}_j \pm \frac{d}{2}\hat{\mathbf{x}}_j$. Then the total interaction energy between two dipolar molecules is given by $U_{ij}^{\text{total}} = U_{ij}^{\text{GB}} + U_{ij}^{\text{dd}}$. Here we have first investigated the phase behavior of the system for different values of the dipolar separation parameter d^* while keeping the dipole strength $\mu^* (\equiv \mu/\sqrt{\epsilon_0\sigma_0^3})$ at a fixed moderate value and then investigated the phase behavior for different values of the dipole strength while keeping the dipolar separation at a fixed moderate value. The dipole moments $\mu^* = 0.3$ and 0.9 , for a molecular diameter of $\sigma_0 \approx 10$ Å and an energy term $\epsilon_0 = 5 \times 10^{-15}$ erg, correspond to 0.67 and 2 D, respectively. The long range dipole-dipole interaction energy has been evaluated using the reaction field [33] method with dipolar cutoff radius $r_{RF}^* \equiv r_{RF}/\sigma_0 = 3.2$ and conducting boundary conditions with dielectric constant $\epsilon_{RF} = \infty$ for the system of $N = 1500$ dipolar molecules. The reaction field technique has been satisfactorily employed in previous simulation studies of ferroelectric phases [34,35]. In our previous work [26], the robustness of the results of the reaction field method was also verified by the computationally expensive Ewald sum method [33].

III. SIMULATION PROCEDURE

Monte Carlo (MC) simulation studies have been performed in the isothermal-isobaric (constant N - P - T) ensemble with periodic boundary conditions imposed on systems of $N = 1500$ and $N = 500$ dipolar ellipsoids. We have performed a cooling sequence of simulation runs along an isobar at a fixed pressure $P^* (\equiv P\sigma_0^3/\epsilon_0) = 100$. A MC simulation of the system of GB ellipsoids without dipoles yielded discotic nematic and hexagonal columnar phases at the same pressure without any ferroelectric order [22].

We started the simulation from a well equilibrated isotropic liquid phase in a cubic box. We then reduced the temperature $T^* (\equiv K_B T/\epsilon_0)$ of the system sequentially to explore the phase behavior. At a given temperature, the final equilibrated configuration obtained from the previous higher temperature was used as the starting configuration. The system was subjected to equilibrium runs of $\geq 5 \times 10^5$ MC cycles at each state point $[p^*, T^*]$. During a MC cycle, each particle was randomly displaced and reoriented following Metropolis criteria where the reorientation moves were performed using Barker-Watts technique [33]. An attempt to change the volume of the cubic box was also performed in each MC cycle.

In addition, some studies were performed using orthogonal boxes to generate more ordered columnar or biaxial phases.

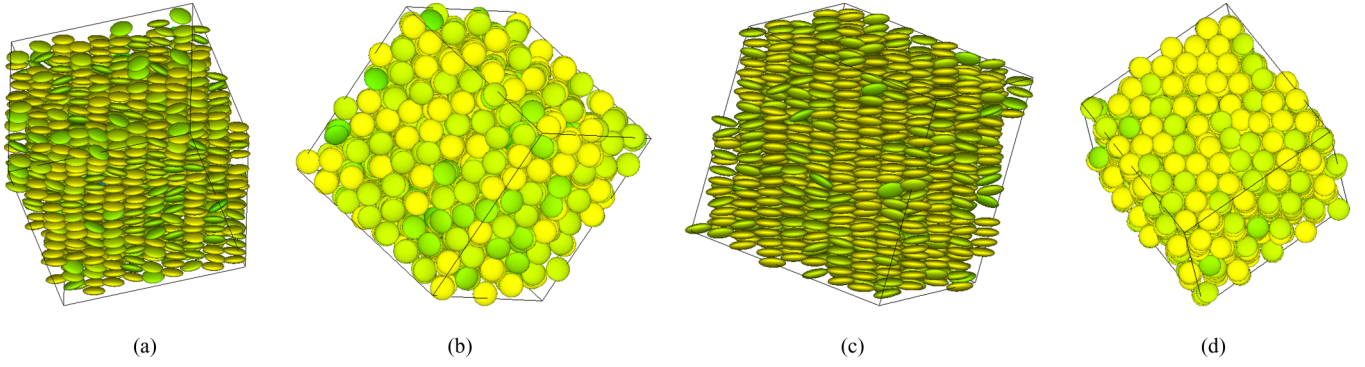


FIG. 1. (Color online) Snapshots of the FCol phases generated by the MC simulations of 1500 dipolar oblate GB molecules for different dipolar separations at a fixed pressure $P^* = 100$ and fixed dipole strength $\mu^* = 0.60$. (a) Side view of the FCol phase showing fluidlike positional ordering along the columns at $(d^* = 0.20, T^* = 9.50)$. (b) Top view of the FCol phase with strong overall polarization at $(d^* = 0.20, T^* = 9.50)$. (c) Side view of the FCol phase with strong overall polarization at $(d^* = 0.30, T^* = 7.50)$. (d) Top view of the FCol phase with hexagonal packing of polarized columns at $(d^* = 0.30, T^* = 7.50)$. The particles are color-coded according to their orientation with respect to the overall polarization vector, ranging from parallel [yellow (light gray)] to antiparallel [dark blue (dark gray)] [37]. In the above configurations, nearly all oblate ellipsoids are colored in yellow (light gray) or some light shade of green (gray) to indicate that the ellipsoids are approximately oriented parallel to the overall polarization vector. The snapshots were generated using the graphics software QMGA [38].

The acceptance ratios of the roto-translational moves and volume moves were adjusted to 40%. To overcome any possibility of locking in a metastable state, the particles were also allowed to attempt up-down flip moves exchanging the particle tip with the bottom with a 20% frequency with respect to the roto-translational MC moves.

IV. RESULTS AND DISCUSSIONS

The average orientational order of the particles was monitored by the second-rank orientational order parameter P_2 defined by the largest eigenvalue of the order tensor $S_{\alpha\beta} = \frac{1}{N} \sum_{i=1}^N \frac{1}{2}(3u_{i\alpha}u_{i\beta} - \delta_{\alpha\beta})$, where $\alpha, \beta = x, y, z$ are the

indices referring to three components of the unit vector $\hat{\mathbf{u}}$ along the orientation of the particles and $\delta_{\alpha\beta}$ is the Kronecker delta. The eigenvector associated with the largest eigenvalue defines the primary director. The value of P_2 is close to zero in the isotropic phase and tends to 1 in the highly ordered phases. The global ferroelectric order was measured by calculating the average polarization per particle P_1 defined by $P_1 = \frac{1}{N} \sum_{i=1}^N \hat{\boldsymbol{\mu}}_i \cdot \hat{\mathbf{d}}$, where $\hat{\mathbf{d}}$ is the unit vector along the direction of total macroscopic moment $\mathbf{P} = \sum_{i=1}^N \boldsymbol{\mu}_i$ and N is the number of molecules in the system. P_1 can be alternatively defined by $P_1 = \frac{1}{N\mu} |\mathbf{P}|$. P_1 is unity in a perfectly ferroelectric phase and zero in an antiferroelectric phase and in the isotropic phase. P_2 is therefore the indicator of global orientational order, and P_1 is the indicator of global ferroelectric order.

We have also measured the biaxial order parameter $\langle R_{2,2}^2 \rangle = \langle \frac{1}{2}(1 + \cos^2 \beta) \cos 2\alpha \cos 2\gamma - \cos \beta \sin 2\alpha \sin 2\gamma \rangle$ as described in [36], where α, β, γ are the Euler angles giving the orientation of the molecular body set of axes with respect to the director set of axes. In a biaxial phase, the anisotropic molecules exhibit additional orientational order along a second macroscopic direction perpendicular to the primary director. This means that we can define a set of perpendicular macroscopic axes of preferential orientation (only two need to be defined as the third is then specified as perpendicular to the other two) in a biaxial phase. In the present system, the symmetry axes of the ellipsoids remain aligned in both the uniaxial and biaxial ferroelectric discotic phases, but the molecular x axes (axes along the separation between two dipoles on each ellipsoid) and molecular y axes (axes perpendicular to both the molecular symmetry axis and the molecular x axis) are significantly oriented only in a biaxial phase. The biaxial order parameter $\langle R_{2,2}^2 \rangle$ measures the degree of ordering of the molecular x and y axes in a plane perpendicular to the primary director [36]. For $\langle P_2 \rangle = 1$, $\langle R_{2,2}^2 \rangle = 0$ the system is perfectly uniaxial, and for $\langle P_2 \rangle = 1$, $\langle R_{2,2}^2 \rangle = 1$ the system is perfectly biaxial.

In order to verify the fluidity of the ferroelectric phases, we calculated the mean square displacement (MSD) as follows:

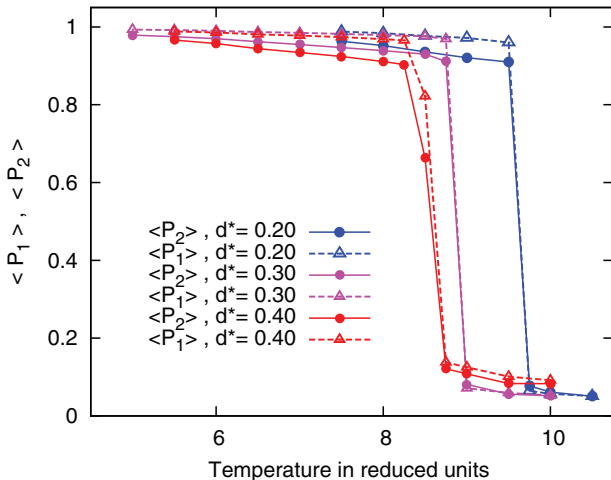


FIG. 2. (Color online) Evolution of the polar order parameter $\langle P_1 \rangle$ and the second-rank order parameter $\langle P_2 \rangle$ against reduced temperature T^* at different dipolar separations: $d^* = 0.20$ ($N = 1500$), 0.30 ($N = 1500$), and 0.40 ($N = 500$). The dashed lines with triangles show $\langle P_1 \rangle$, and the solid lines with circles show $\langle P_2 \rangle$. All the results are for constant pressure $P^* = 100.0$ and fixed dipole strength $\mu^* = 0.60$. Different colors are used for different dipolar separations d^* , as described in the legend.

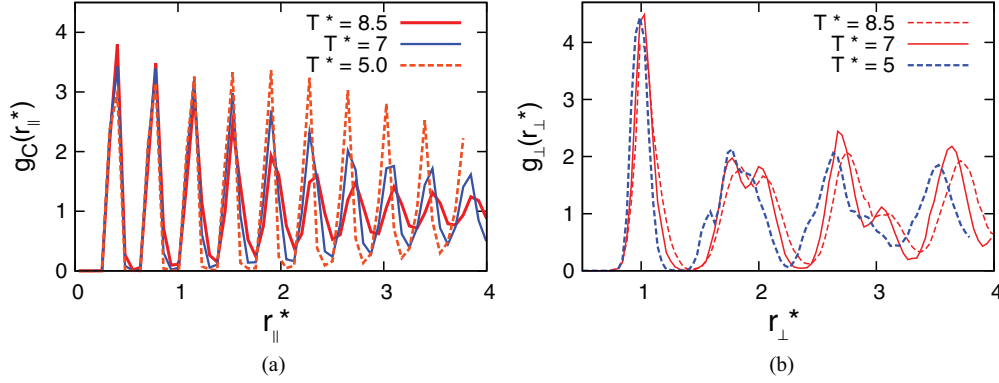


FIG. 3. (Color online) (a) Columnar distribution function $g_c(r_{\parallel}^*)$ at $(\mu^* = 0.60, d^* = 0.30, N = 1500)$ for three different temperatures: $T^* = 8.5, 7.0$, and 5.0 . (b) Perpendicular distribution function $g_{\perp}(r_{\perp}^*)$ at $(\mu^* = 0.60, d^* = 0.30, N = 1500)$ for three different temperatures: $T^* = 8.5, 7.0$, and 5.0 .

$\langle R^2 \rangle_{\tau} = \frac{1}{N} \sum_{i=1}^N [\mathbf{r}_i(\tau) - \mathbf{r}_i(0)]^2$, where $\mathbf{r}_i(\tau)$ is the position vector of the i th particle after completion of τ MC cycles. In the fluid phases, the mean square displacement steadily increases with increasing τ , indicating fluid behavior. In contrast for solids $\langle R^2 \rangle_{\tau}$ becomes constant as τ increases. For a proper structural analysis of the resultant ferroelectric phases, we calculated important distribution functions as required. We have measured the radial distribution function $g(r) = \frac{1}{4\pi r^2 \rho} \langle \delta(r - r_{ij}) \rangle_{ij}$, where the average is taken over all the molecular pairs. The columnar distribution function $g_c(r_{\parallel}^*)$ and the perpendicular distribution function $g_{\perp}(r_{\perp}^*)$ for the disklike ellipsoids are calculated following [30].

A system consisting of GB disks without any dipoles forms isotropic (I), discotic nematic (N), and columnar (Col) hexagonal phases for the same set of GB parameters used here [22]. Here two axial off-center parallel point dipole moments are symmetrically placed on the equatorial plane of the ellipsoids to generate liquid crystal phases with a strong global polarization.

A. Influence of the dipolar separation

We have investigated the liquid crystalline phase behavior exhibited by systems of polar disks for different values of

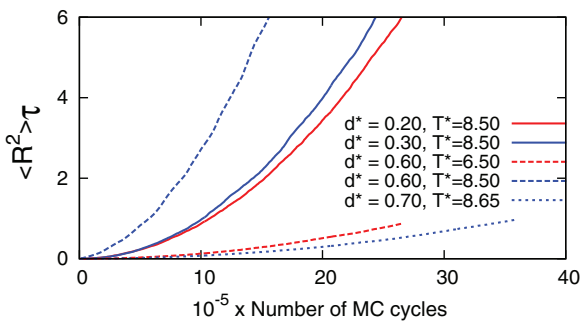


FIG. 4. (Color online) Mean square displacement $\langle R^2 \rangle_{\tau}$ against MC cycles for the FNLC phase at $(T^* = 8.5, d^* = 0.60)$, ferroelectric hexagonal columnar phases at $(T^* = 8.5, d^* = 0.20)$ and $(T^* = 8.5, d^* = 0.30)$, and ferroelectric biaxial phases at $(T^* = 8.5, d^* = 0.60)$ and $(T^* = 8.65, d^* = 0.70)$ as obtained for $N = 1500$ dipolar particles.

the dipolar separation d^* in the range $0.20 \leq d^* \leq 0.70$, where d^* is varied in steps of $\Delta d^* = 0.10$. The simulation results show that the separation between two symmetrically positioned dipoles on the disk shaped ellipsoids can profoundly influence the phase behavior of the system. The MC N - P - T simulations for different dipolar separations are performed with a fixed dipole strength $\mu^* = 0.60$ and a fixed reduced pressure $P^* = 100$. For smaller dipolar separations ($d^* = 0.20$ and 0.30), the systems exhibit isotropic and ferroelectric ($\langle P_1 \rangle > 0$) columnar phases. No nematic phase is obtained for these dipolar separations. Starting with isotropic liquids, the ferroelectric columnar phases are obtained via strong isotropic to ferroelectric columnar transitions. All the columnar phases consist of strongly polarized columns. Snapshots of the ferroelectric columnar phases obtained for smaller dipolar separations are given in Fig. 1. The variations of the average order parameters $\langle P_1 \rangle, \langle P_2 \rangle$ against the reduced temperature T^* are shown in Fig. 2. The strong stabilization of a columnar fluid with polarized columns at high temperatures can be considered to be the effect of strong head-to-tail dipolar interactions among the ellipsoids inside each column. The isotropic-ferroelectric columnar transition gradually shifts to a lower temperature with increasing d^* , which is an indication that the strength of head-to-tail dipolar interactions is reduced for higher dipolar separations. On the other hand, the formation of ferroelectric columnar phases with strong overall polarization ($\langle P_1 \rangle \approx 1$) for $d^* = 0.20, 0.30$ can be considered to be an indication of stronger column-column interactions that was not possible in the case of single dipolar cut spheres generating antiferroelectric columnar phases [5,16].

For a proper understanding of the columnar structures, we have calculated the required distribution functions. Here we describe the structural features of the columnar phases obtained for $d^* = 0.30$. The structural characteristics of the columnar phases remain qualitatively similar for $d^* = 0.20$ and $d^* = 0.40$. The columnar distribution function $g_c(r_{\parallel}^*)$, which is a measure of positional order within a single column, is shown in Fig. 3(a). The periodic nature of $g_c(r_{\parallel}^*)$ generally confirms the periodic stacking of molecules in the columnar phases. At $T^* = 8.5$, algebraic decay of $g_c(r_{\parallel}^*)$ indicates a fluidlike positional ordering along the columns. As the temperature is lowered, $g_c(r_{\parallel}^*)$ exhibits long range periodic structure.

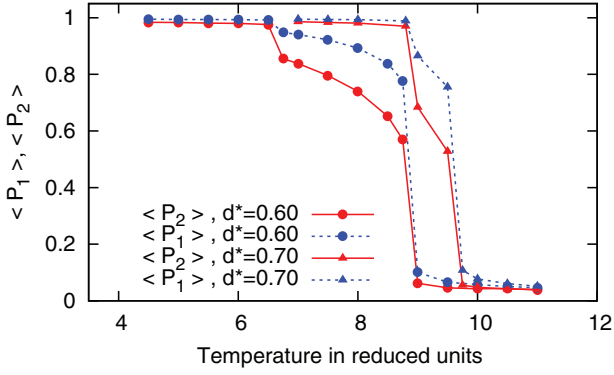


FIG. 5. (Color online) Evolution of the polar order parameter $\langle P_1 \rangle$ and the second-rank order parameter $\langle P_2 \rangle$ against reduced temperature T^* for $d^* = 0.60$ and $d^* = 0.70$ at ($P^* = 100.0$, $\mu^* = 0.60$, $N = 1500$). Solid lines with circles and triangles show $\langle P_2 \rangle$ for $d^* = 0.60$ and 0.70 , respectively. Dashed lines with circles and triangles show $\langle P_1 \rangle$ for $d^* = 0.60$ and 0.70 , respectively.

Figure 3(b) shows the perpendicular distribution function $g_{\perp}(r_{\perp}^*)$, which is a measure of translational order in the plane orthogonal to the orientation of the disk shaped molecules. At $T^* = 8.5$ and 7 , three distinct peaks for $r_{\perp}^* < 2.05$ with a ratio close to $1 : \sqrt{3} : 2$ indicate perfect hexagonal columnar packing. At $T^* = 5.0$, we observed a transformed $g_{\perp}(r_{\perp}^*)$, which is due to increased interdigitation of ellipsoids.

In order to verify the fluidity of the columnar phases, we have measured the mean square displacement of ellipsoids against MC steps as given in Fig. 4. The plots show that these columnar structures are highly fluid as the MSD steadily increases with MC steps. It should be noted that the I-FCol transition temperature is lowered with increasing dipolar separation, as can be seen from the plots in Fig. 2. As the dipolar separation is further increased, the highly desired ferroelectric nematic fluid comes into the picture. A stable ferroelectric nematic (FN) fluid is obtained at $T^* = 8.5$ for $d^* = 0.40$. For $d^* = 0.40$ and 0.50 , we find both the ferroelectric nematic and ferroelectric columnar phases with strong macroscopic polarization. The temperature range of the FN phase increases with d^* . The ferroelectric nematic

and columnar fluids obtained for $d^* = 0.50$ have already been extensively described in our previous paper [26].

Let us now consider the cases of larger dipolar separation $d^* = 0.60$ and 0.70 . The variations of the average order parameters $\langle P_1 \rangle, \langle P_2 \rangle$ against the reduced temperature, for $d^* = 0.60$ and 0.70 , are presented in Fig. 5. It can be seen from Fig. 5 that the temperature range of the ferroelectric nematic fluid reaches a maximum at $d^* = 0.60$ and then decreases at $d^* = 0.70$. Larger dipolar separations are found to strongly stabilize a ferroelectric biaxial (FB) phase. Figure 6(a) shows the radial distribution function $g(r^*)$ at different temperatures for $d^* = 0.60$. The flatness in $g(r^*)$ at $T^* = 8.5$ and 7 reflects the structurelessness of the ferroelectric nematic liquid. At $T^* = 8.5$ and 7 , $g_c(r_{\parallel}^*)$ and $g_{\perp}(r_{\perp}^*)$ show no sign of any long range of positional order as shown in Figs. 6(b)–6(c). The small peaks for $r^*, r_{\parallel}^* < 0.5$ in $g_c(r_{\parallel}^*)$ and in $g(r^*)$ describe the finite probability of short range face-to-face ordering in the FNLC phase. Considerable structure in $g(r^*)$ at $T^* \leq 6.5$ indicates the formation of the more ordered biaxial phase. Snapshots of the ferroelectric nematic phase and the ferroelectric biaxial phase obtained for $d^* = 0.60$ are shown in Fig. 7. We have measured the conventional biaxial order parameter $\langle R_{2,2}^2 \rangle$, which is considered to be a significant measure of the phase biaxiality. The value of the biaxial order parameter is $\langle R_{2,2}^2 \rangle \approx 1$, as measured in the biaxial phases. However, $\langle R_{2,2}^2 \rangle \approx 0$ in the ferroelectric nematic and columnar phases described so far.

From the snapshots of the biaxial phases as given in Figs. 7(b)–7(d), we can get some understanding of the related structures. It can be seen that the ellipsoids are arranged such that the separation vectors between the dipoles on them acquire a global orientational order. This ordering can be understood as the effect of strong dipolar pair interaction that is possible in this situation between dipoles of neighboring ellipsoids if the dipoles are placed very near each other. Snapshots of such arrangement are shown in Figs. 7(b)–7(d). The structural distribution functions calculated for the biaxial phase are different from that of the columnar phases described before. At $T^* = 6.5$ and 4.5 , $g_c(r_{\parallel}^*)$ indicates the intercalated arrangement of the ellipsoids. The sharp peaks in $g_c(r_{\parallel}^*)$ come from molecules sitting above each other with their separation vector oriented along their symmetry axes. The

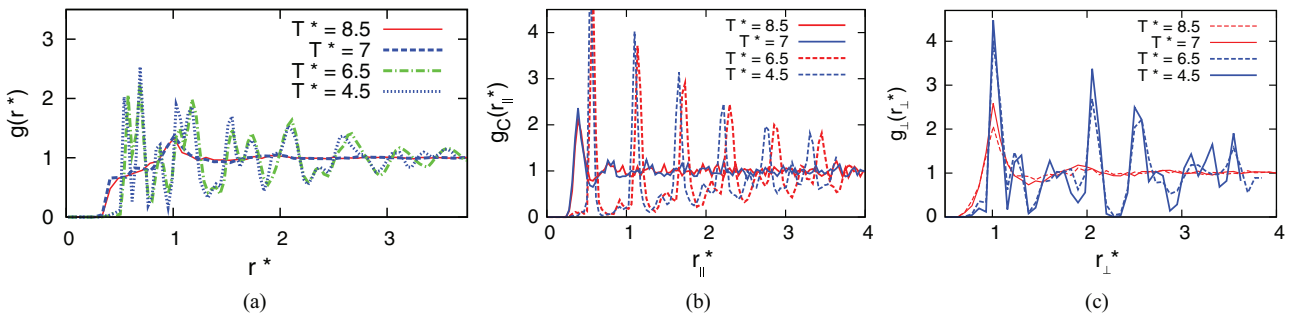


FIG. 6. (Color online) Structural distribution functions for $\mu^* = 0.60, d^* = 0.60$. (a) Radial distribution function $g(r^*)$ at four different temperatures: $T^* = 8.5$ (FNLC), $T^* = 7.0$ (FNLC), $T^* = 6.5$ (FB), $T^* = 4.5$ (FB). (b) Columnar distribution function $g_c(r_{\parallel}^*)$ at four different temperatures: $T^* = 8.5$ (FNLC), $T^* = 7.0$ (FNLC), $T^* = 6.5$ (FB), $T^* = 4.5$ (FB). (c) Perpendicular distribution function $g_{\perp}(r_{\perp}^*)$ at four different temperatures: $T^* = 8.5$ (FNLC), $T^* = 7.0$ (FNLC), $T^* = 6.5$ (FB), $T^* = 4.5$ (FB). FNLC stands for ferroelectric nematic liquid crystal phase, and FB stands for ferroelectric biaxial phase.

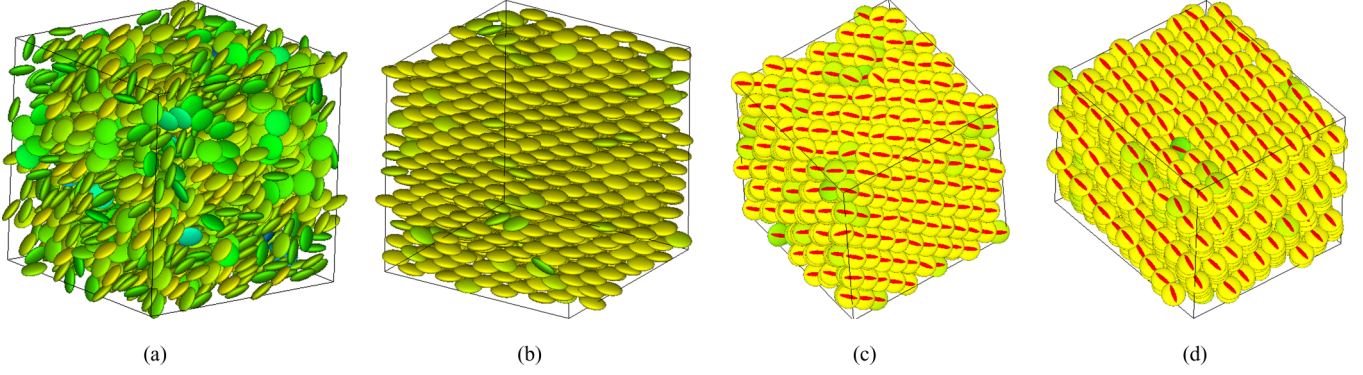


FIG. 7. (Color online) Snapshots of the configurations generated by MC simulations for $\mu^* = 0.60, d^* = 0.60$. (a) FNLC phase at $T^* = 8.5$ with strong ferroelectric order. (b) Arrangement of the disk shaped molecules in the biaxial phase with strong overall polarization at $T^* = 6.5$. (c) A top view of the highly ordered biaxial ferroelectric phase obtained at $T^* = 6.5$, where the dipolar separation vectors on the ellipsoids are indicated by red (gray) lines. (d) Highly ordered biaxial ferroelectric phase obtained at $T^* = 8.0$ for $(\mu^* = 0.60, d^* = 0.70)$, where the orientations of the dipolar separation vectors of the ellipsoids are indicated by red (gray) lines. The ellipsoids are color-coded according to their orientation with respect to the overall polarization vector, ranging from parallel [yellow (light gray)] to antiparallel [dark blue (dark gray)] [37]. In (b),(c) and (d), nearly all oblate ellipsoids are colored in yellow (light gray) or some light shade of green (gray) to indicate that the ellipsoids are approximately oriented parallel to the overall polarization vector. In (a), the presence of a large number of green (gray) colored ellipsoids indicate comparatively weaker ferroelectric order with respect to that in (b),(c) and (d).

separation between two consecutive peaks in $g_c(r_{11}^*)$ is much higher than that in a columnar phase because of the biaxial arrangement. In order to verify the fluidity of the ferroelectric nematic and biaxial phases, we have measured the mean square displacements of ellipsoids against MC steps as given in Fig. 4. The plots show that the ferroelectric nematic structures are highly fluid as the MSD steadily increases with MC steps but the molecules in the biaxial phase exhibit much slower diffusion. So the ferroelectric biaxial phase is more of a solidlike phase. Higher dipolar separations strongly stabilize the ferroelectric biaxial phase by destabilizing all other phases. However, the ferroelectric nematic fluids obtained at these higher dipolar separations show no sign of global biaxial order. The FN-FB transition occurs at higher temperature for $d^* = 0.70$ with respect to that for $d^* = 0.60$. For $d^* = 0.80$ there is a high probability of sticking of the ellipsoids as the

terminal dipoles of neighboring ellipsoids can become very close to each other.

In order to understand the phase behavior described above, it is useful to examine how the pair interaction, especially the electrostatic part of the interaction, varies with the dipolar separation d^* . The pair interaction energy between two dipolar ellipsoids and the electrostatic part of the interaction are plotted in Figs. 8(a) and 8(b), respectively, as a function of the component of the pair separation vector \mathbf{r} perpendicular to the particle symmetry axes r_{\perp}^* as one particle is slid over the other while maintaining a fixed separation ($r_{\parallel} = \sigma_e$) along the symmetry axis and having all dipoles oriented in the same direction. Note that when r_{\perp}^* is zero, one particle completely covers the other. Curves are shown for different dipolar separations. Here we have discussed the case where the ellipsoid is sliding along the direction of the molecular x

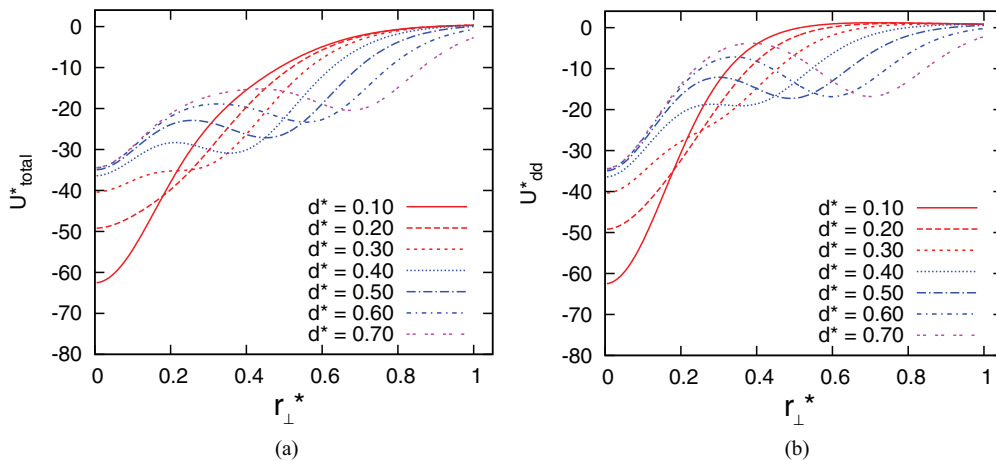


FIG. 8. (Color online) Variations of (a) total pair interaction energy U_{total}^* and (b) the electrostatic part of the pair interaction energy U_{dd}^* of two polar ellipsoids with parallel dipolar separation vectors as one polar ellipsoid is slid over another along the dipolar separation vector with their dipoles oriented in the same direction while keeping the component of the interparticle vector parallel to the symmetry axes of the particles at a fixed value of σ_e . r_{\perp}^* is the component of the interparticle vector perpendicular to the symmetry axes of the particles. In all cases, $\mu^* = 0.60$. The different curves are for $d^* = 0.10, 0.20, 0.30, 0.40, 0.50, 0.60,$ and 0.70 , as described in the legend.

axis, i.e., along the dipolar separation vector \mathbf{d}^* ($= d^*\hat{x}$) of the ellipsoids. This particular case is important for the biaxial phase behavior discussed above in the cases of $d^* = 0.60$ and $d^* = 0.70$.

It is evident from Fig. 8(b) that the dipolar separation has a dramatic effect on the pair potential. For smaller values of d^* , the strong head-to-tail dipolar interaction results in sharper minima at $r_{\perp}^* = 0$. It is the sharpness of this potential which leads to columnar order and destabilization of the nematic phase for $d^* \leq 0.30$. As the dipoles become farther separated, the dipolar interaction loses its sharp focus and generates a weaker and slowly varying attraction which helps in generating the ferroelectric nematic phase. It can be seen that for a separation $d^* \geq 0.50$, a prominent second well is constructed with its minimum at $r_{\perp}^* = d^*$. Therefore the position of the minimum of the second well shifts with the dipolar separation. The second well simply results from the interaction between two parallel dipoles when they are positioned above each other. This interaction helps to stabilize the ferroelectric biaxial phase. In the uniaxial ferroelectric nematic and the uniaxial ferroelectric columnar phases, the dipolar separation vectors of two neighboring ellipsoids are usually randomly oriented with respect to each other. In such cases, the pair interaction generates a sharp attractive well for smaller d^* and a weaker, flatter attraction for larger d^* , but there is no second well as found for parallel orientation of the dipolar separation vectors of the two ellipsoids. The behavior of the pair interaction thus satisfactorily supports the overall phase behavior.

B. Influence of the dipole strength

We have performed MC N - P - T simulations at different dipole strengths in the range $0.30 \leq \mu^* \leq 0.90$ for a fixed dipolar separation $d^* = 0.50$. The dipole strength is varied in steps of $\Delta\mu^* = 0.10$. For $\mu^* = 0.30$, the dipolar interactions remain too weak to generate a global ferroelectric order at higher temperatures. The nematic and columnar fluids without any global polarization appear at $T^* = 6.25$ and 5.5 , respectively, as the temperature is reduced. At temperatures $T^* \leq 4.75$, the average polar order parameter $\langle P_1 \rangle$ increases from $\langle P_1 \rangle \approx 0.1$ with the decrease in temperature, as shown in Fig. 9(a). At $T^* = 3.5$, a columnar phase with strong overall polarization ($\langle P_1 \rangle \approx 1$) is obtained. Figures 10(a) and 10(b) show snapshots of the columnar phases obtained at $T^* = 5.5$ and 3.5 , respectively. It is seen that at the higher temperature, the columns are partially polarized, which results in weak overall polarization. However, at $T^* = 3.5$, a strongly polarized ferroelectric columnar phase is obtained with $N = 1500$ particles. The variation of the average order parameters against the reduced temperature T^* for different dipole strengths is described in Fig. 9.

For higher dipole strengths ($\mu^* = 0.40, 0.50$), a global ferroelectric order is successfully generated in both the nematic and columnar fluids. The phase behavior remains qualitatively similar for these dipole strengths except that the ordered phases appear at higher temperatures for higher dipole strengths as the stronger dipolar interaction always prefers more ordered phases. Snapshots of the ferroelectric nematic and columnar phases obtained for $\mu^* = 0.40$ are shown in Figs. 10(c) and 10(d). From Fig. 10(d), it can be seen that there is a fluidlike positional ordering along the columns at $T^* = 6.0$.

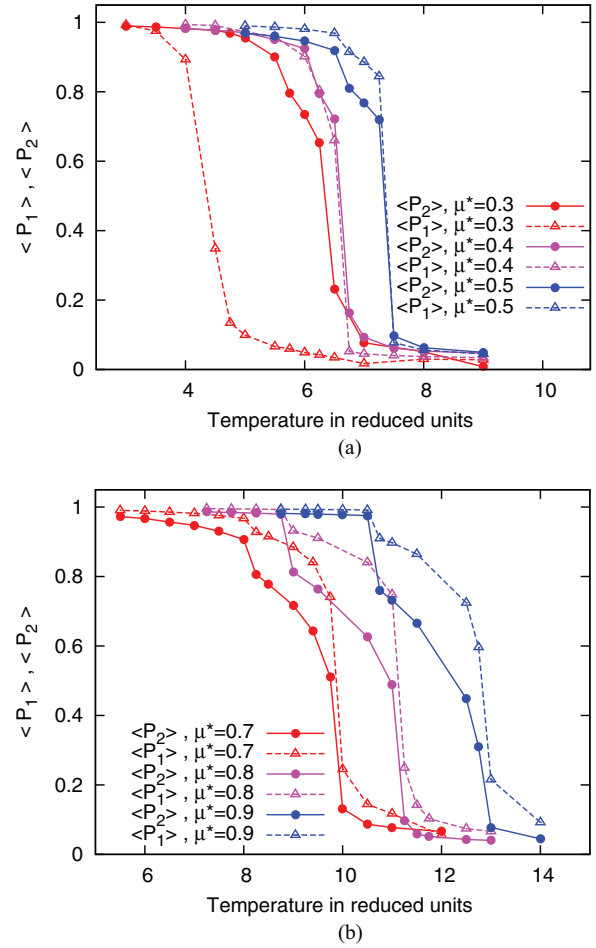


FIG. 9. (Color online) Evolution of the polar order parameter $\langle P_1 \rangle$ and the second-rank order parameter $\langle P_2 \rangle$ against reduced temperature T^* at different dipole strengths: (a) $\mu^* = 0.30$ ($N = 1500$), 0.40 ($N = 1500$), 0.50 ($N = 1500$) and (b) $\mu^* = 0.70$ ($N = 500$), 0.80 ($N = 1500$), 0.90 ($N = 1500$). The dashed lines with triangles show $\langle P_1 \rangle$, and the solid lines with circles show $\langle P_2 \rangle$. All the results are for constant pressure $P^* = 100.0$ and fixed dipole separation $d^* = 0.50$. Different colors are used for different dipole strengths μ^* as described in the legend.

The important structural distribution functions are presented in Figs. 11(a)–11(c) for different ferroelectric phases obtained with $\mu^* = 0.40$. The flatness in $g(r^*)$, $g_c(r_{\parallel}^*)$, and $g_{\perp}(r_{\perp}^*)$ at $T^* = 6.5$ confirms the structurelessness of the ferroelectric nematic liquid. Considerable structure in $g(r^*)$ at $T^* = 6.0$ and 4.0 indicates the formation of columnar phases. At $T^* = 6.0$, $g_c(r_{\parallel}^*)$ decays rapidly, indicating a fluidlike ordering along the columns. As the temperature is further lowered, $g_c(r_{\parallel}^*)$ exhibits long range periodic structure. The small peaks for $r_{\parallel}^*, r^* < 0.5$ in $g_c(r_{\parallel}^*)$ and in $g(r^*)$ describe the finite probability of short range face-to-face ordering in the FNLC phase at $T^* = 6.5$. At $T^* = 6.0$, a flat second peak in $g_{\perp}(r_{\perp}^*)$ indicates less perfect hexagonal columnar packing. At $T^* = 4.0$, $g_{\perp}(r_{\perp}^*)$ indicates increased interdigitation of ellipsoids.

In order to confirm the fluidity of the columnar phases, we have also measured the mean square displacement as described before, and the results show that the ferroelectric

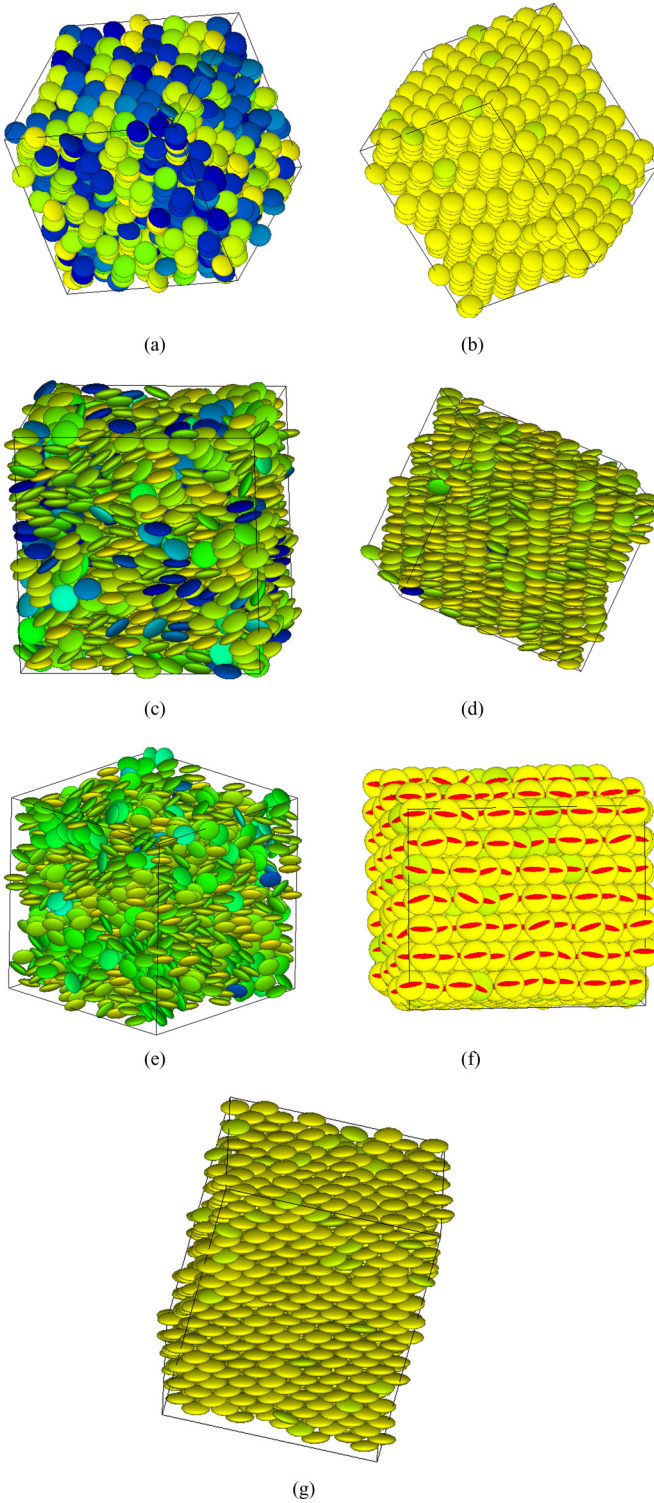


FIG. 10. (Color online) Snapshots of the interesting configurations generated by MC simulations at different dipole strengths for a fixed dipolar separation $d^* = 0.50$. (a) FCol phase at $(T^* = 5.5, \mu^* = 0.30)$ with partially polarized columns and weak overall polarization. (b) FCol phase at $(T^* = 3.5, \mu^* = 0.30)$ with strong overall polarization. (c) FNLC phase at $(T^* = 6.0, \mu^* = 0.40)$ with fluidlike positional order along the columns. (d) FCol phase at $(T^* = 6.5, \mu^* = 0.40)$. (e) FNLC phase at $(T^* = 11, \mu^* = 0.80)$. (f) FB phase at $(T^* = 8.75, \mu^* = 0.80)$. The orientations of the dipolar separation vectors (directed from one dipole to the other of each ellipsoid)

nematic and hexagonal columnar structures are highly fluid as the MSD steadily increased with MC steps. The phase behavior for $\mu^* = 0.60$ was demonstrated in our previous work [26]. For $\mu^* = 0.50, 0.60,$ and 0.70 , the systems exhibit ferroelectric nematic and hexagonal columnar phases with strong overall polarization where the temperature range of the ferroelectric nematic phase increases with dipole strength. Let us now describe the phase behavior for higher dipole strengths $\mu^* = 0.80$ and 0.90 . The systems exhibit ferroelectric nematic and ferroelectric biaxial phases. No ferroelectric columnar phase is obtained at these dipole strengths. The temperature range of the ferroelectric nematic phase increases for these dipole strengths. Snapshots of the ferroelectric nematic and the ferroelectric biaxial phases obtained for $\mu^* = 0.80$ are shown in Figs. 10(e)–10(g). Figure 11(d) shows the radial distribution function $g(r^*)$ at different temperatures for $\mu^* = 0.80$. The flatness in $g(r^*)$ at $T^* = 11.0$ and 9.0 reflects the structurelessness of the ferroelectric nematic liquid in the long range. At $T^* = 11.0$ and 9 , $g_c(r_{||}^*)$ and $g_{\perp}(r_{\perp}^*)$ also show no sign of any long range of positional order. The small peaks for $r_{||}^*, r_{\perp}^* < 0.5$ in $g_c(r_{||}^*)$ and in $g(r^*)$ describe the finite probability of short range face-to-face ordering in the FNLC phase. Considerable structure in $g(r^*)$ at $T^* \leq 8.75$ indicates the formation of a more ordered biaxial phase.

We have also measured the conventional biaxial order parameter $\langle R_{2,2}^2 \rangle$, the value which is ≈ 1 as measured in all the biaxial phases. However, $\langle R_{2,2}^2 \rangle$ remain ≈ 0.0 in the ferroelectric nematic and columnar phases up to the temperatures reported here. From the snapshots of the biaxial phases, we can understand the related structure. From Fig. 10(f), it can be seen that the dipoles are arranged such that the dipolar separation vectors pointing from one dipole to a disk to the other get oriented mostly in the same direction. This ordering can be understood as the effect of the strong pair interaction possible in this condition between two terminal dipoles of neighboring ellipsoids if two parallel dipoles are placed above each other. A snapshot of such an intercalated arrangement is shown in Fig. 10(g). The structural distribution functions for the biaxial phase are shown in Figs. 11(d)–11(f). At $T^* = 8.75$ and 7.25 , $g_c(r_{||}^*)$ indicates the intercalated arrangement of the ellipsoids. The shorter peaks generate due to the presence of the pairs of side-by-side ellipsoids covering single ellipsoids. As the plots of pair interaction showed that the minimum of the second well is positioned at $r_{\perp}^* = d^*$, these shorter peaks cannot be observed in the columnar distribution function of the biaxial phases for $d^* = 0.60$ and 0.70 . It should be noted that strong dipoles stabilize ferroelectric nematic phases with relatively weak orientational order. We have measured the mean square displacement as described before, and the results show that the ferroelectric nematic phases obtained for stronger dipolar strengths are highly fluid, but the biaxial phases showed

FIG. 10. (Continued) are indicated by red (gray) lines. (g) Intercalated arrangement of the disk shaped molecules in the ferroelectric biaxial phase at $T^* = 8.75, \mu^* = 0.80$. The particles are color-coded according to their orientation with respect to the overall polarization vector, ranging from parallel [yellow(light gray)] to antiparallel [dark blue (dark gray)] [37].

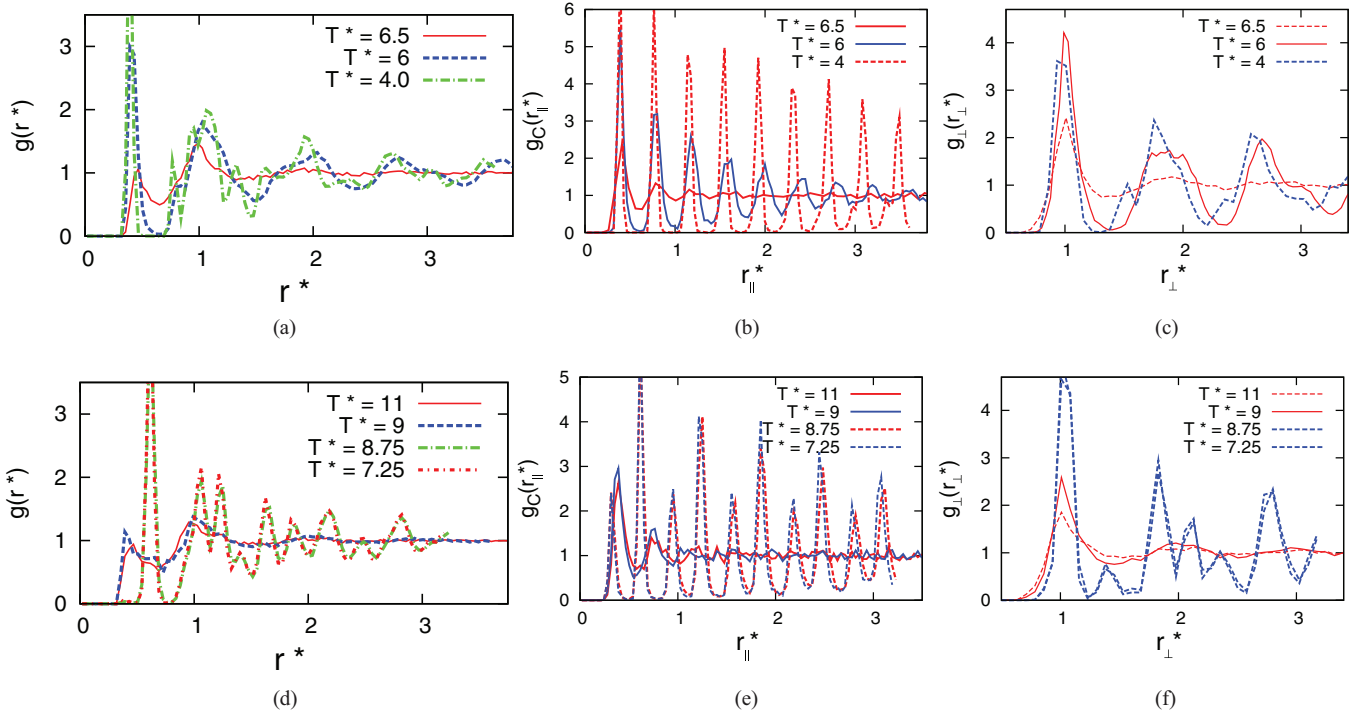


FIG. 11. (Color online) (a)–(c) Structural distribution functions for $(\mu^* = 0.40, d^* = 0.50)$. (a) Radial distribution function $g(r^*)$ at three different temperatures: $T^* = 6.5$ (FNLC), $T^* = 6.0$ (FCol), $T^* = 4.0$ (FCol). (b) Columnar distribution function $g_c(r_{\parallel}^*)$ at three temperatures: $T^* = 6.5$, $T^* = 6.0$, $T^* = 4.0$. (c) Perpendicular distribution function $g_{\perp}(r_{\perp}^*)$ at three temperatures: $T^* = 6.5$, $T^* = 6.0$, $T^* = 4.0$. (d)–(f) Structural distribution functions for $(\mu^* = 0.80, d^* = 0.50)$. (d) Radial distribution function $g(r^*)$ at four different temperatures: $T^* = 11$ (FNLC), $T^* = 9.0$ (FNLC), $T^* = 8.75$ (FB), $T^* = 7.25$ (FB). (e) Columnar distribution function $g_c(r_{\parallel}^*)$ at four temperatures: $T^* = 11$, $T^* = 9.0$, $T^* = 8.75$, $T^* = 7.25$. (f) Perpendicular distribution function $g_{\perp}(r_{\perp}^*)$ at four temperatures: $T^* = 11$, $T^* = 9.0$, $T^* = 8.75$, $T^* = 7.25$. FNLC stands for ferroelectric nematic liquid crystal phase, FCol stands for ferroelectric columnar liquid crystal phase, and FB stands for ferroelectric biaxial phase.

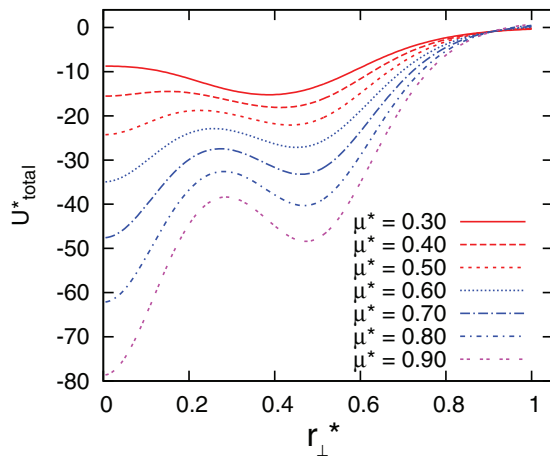


FIG. 12. (Color online) Variation of the pair interaction energy U_{total}^* of two polar ellipsoids with parallel dipolar separation vectors as one polar ellipsoid is slid over another along the dipolar separation vector with their dipoles oriented along their symmetry axes and while keeping the component of the interparticle vector parallel to the symmetry axes of the particles at a fixed value of σ_e . r_{\perp}^* is the component of the interparticle vector perpendicular to the symmetry axes of the particles. In all cases, $d^* = 0.50$. The different curves are for $\mu^* = 0.30, 0.40, 0.50, 0.60, 0.70, 0.80$, and 0.90 as described in the legend.

much slower diffusion of the ellipsoids. It should also be noted that higher dipolar strengths progressively stabilize the ferroelectric biaxial phase by destabilizing all other phases. The ferroelectric nematic to ferroelectric biaxial transition occurs at higher temperature for $\mu^* = 0.90$ with respect to that for $\mu^* = 0.80$.

In order to understand the phase behavior described above, it is useful to examine the variation of the pair interaction with dipole strength. In Fig. 12 the reduced pair potential of two dipolar ellipsoids is plotted as a function of the component of the pair separation vector \mathbf{r} perpendicular to the particle symmetry axes r_{\perp}^* as one particle is slid over the other while maintaining a fixed separation ($r_{\parallel} = \sigma_e$) along the symmetry axis and having all dipoles oriented in the same direction. Note that when r_{\perp}^* is zero, one particle completely covers the other. Here we again discuss the case where the ellipsoid is sliding along the direction of the molecular x axis, i.e., along the dipolar separation vector $\mathbf{d}^* (= d^* \hat{x})$ of the ellipsoids. Curves are shown for different dipolar strengths. It is evident from Fig. 12 that as the dipolar strength is increased, the pair potential generates stronger attraction with deeper wells as described before during the variation of dipolar separation. The slowly varying attraction results in the ferroelectric nematic phase for the different dipole strengths studied here. The strengthening of the second well favors strong stabilization of the ferroelectric biaxial phase at higher dipole strengths.

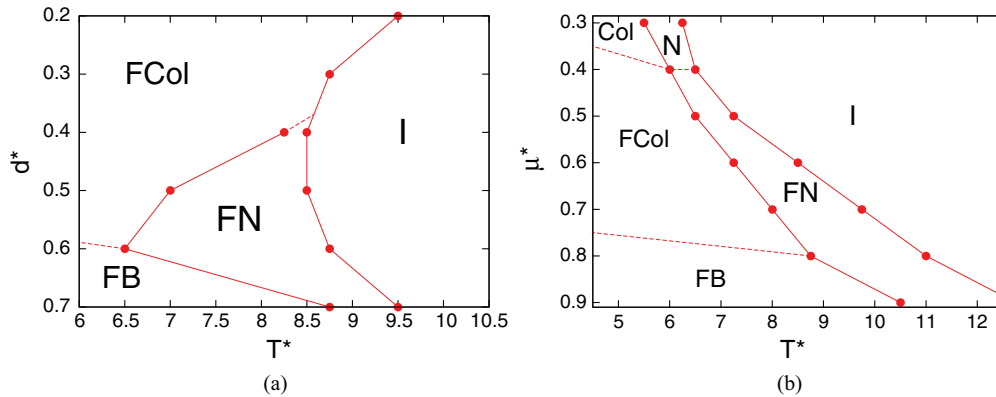


FIG. 13. (Color online) Approximate phase diagrams for the model polar disks. The phases indicated are the isotropic (I), ferroelectric nematic (FN), ferroelectric columnar (FCol), ferroelectric biaxial (FB), apolar nematic (N), and apolar columnar (Col) phases. (a) (T^*, d^*) diagram at $(P^* = 100, \mu^* = 0.60)$. (b) (T^*, μ^*) diagram at $(P^* = 100, d^* = 0.50)$.

V. SIMPLE PHASE DIAGRAMS

The results are conveniently summarized in the simple and approximate phase diagrams given in Fig. 13. Here we have plotted phase boundaries on (T^*, d^*) and (T^*, μ^*) diagrams, and the stable phase in each region is indicated. The higher temperatures are chosen to emphasize ferroelectric nematic and ferroelectric columnar fluid regions. The phase boundary lines are obtained by examining the order parameters and structural distribution functions. We emphasize that these lines were not obtained from rigorous thermodynamic calculations and are therefore approximate.

VI. CONCLUSIONS

The present model exhibits a rare collection of proper ferroelectric liquid crystal phases of dipolar origin in systems of anisotropic molecules even in the absence of any noncentrosymmetric geometry or chirality of the constituent molecules, which are usually considered to be the necessary elements for realizing a ferroelectric liquid crystal phase. The purpose of this work has been to demonstrate the influences of the dipolar separation and the dipole strength upon the existence of different ferroelectric phases. We observed that the uniaxial ferroelectric columnar fluid, the uniaxial ferroelectric nematic phase, and the ferroelectric

biaxial phase are stabilized at small, medium, and large dipolar separations for a fixed moderate dipole strength, respectively. When studying the phase behavior for different dipole strengths with a fixed intermediate dipolar separation, we found that strong dipoles stabilize the ferroelectric biaxial phase by destabilizing ferroelectric nematic and columnar phases. The highly desired ferroelectric nematic phase is generated for a wide range of dipole strengths where the temperature range of the ferroelectric nematic phase increases with the dipole strength. This paper offers a more complete understanding of the phase behavior of the model particles that display long searched ferroelectric nematic and columnar phases and is a step towards understanding the suitable conditions for possibly generating ferroelectric nematic or ferroelectric columnar order in systems of disk shaped polar anisotropic molecules. However, a study on the effects of changing the shape anisotropy parameter κ should be performed in the future to gain a full understanding.

ACKNOWLEDGMENTS

T.K.B. gratefully acknowledges the support of CSIR, India, for providing a Senior Research Fellowship via Sanction No. 09/028(0794)/2010-EMR-I. This work was supported by the UGC-UPE scheme of the University of Calcutta and the FIST scheme of DST, India.

-
- [1] L. M. Blinov, *Liq. Cryst.* **24**, 143 (1998).
 - [2] L. A. Beresnev, L. M. Blinov, M. A. Osipov, and S. A. Pikin, *Mol. Cryst. Liq. Cryst.* **158**, 1 (1988).
 - [3] P. Palffy-Muhoray, M. A. Lee, and R. G. Petschek, *Phys. Rev. Lett.* **60**, 2303 (1988).
 - [4] D. Wei and G. N. Patey, *Phys. Rev. Lett.* **68**, 2043 (1992).
 - [5] J. J. Weis, D. Levesque, and G. J. Zarragoicoechea, *Phys. Rev. Lett.* **69**, 913 (1992).
 - [6] D. Wei, G. N. Patey, and A. Perera, *Phys. Rev. E* **47**, 506 (1993).
 - [7] B. Park, J. W. Wu, and H. Takezoe, *Phys. Rev. E* **63**, 021707 (2001).
 - [8] B. Groh and S. Dietrich, *Phys. Rev. Lett.* **72**, 2422 (1994); *Phys. Rev. E* **50**, 3814 (1994).
 - [9] E. M. Terentjev, M. A. Osipov, and T. J. Sluckin, *J. Phys. A* **27**, 7047 (1994).
 - [10] O. Francescangeli, V. Stanic, S. I. Torgova, A. Strigazzi, N. Scaramuzza, C. Ferrero, I. P. Dolbnya, T. M. Weiss, R. Berardi, L. Muccioli, S. Orlandi, and C. Zannoni, *Adv. Funct. Mater.* **19**, 2592 (2009).
 - [11] D. Wei and G. N. Patey, *Phys. Rev. A* **46**, 7783 (1992).
 - [12] J. J. Weis and D. Levesque, *Phys. Rev. E* **48**, 3728 (1993); D. Levesque and J. J. Weis, *ibid.* **49**, 5131 (1994).
 - [13] D. Levesque, J. J. Weis, and G. J. Zarragoicoechea, *Phys. Rev. E* **47**, 496 (1993).
 - [14] A. Gil-Villegas, S. McGrother, and G. Jackson, *Chem. Phys. Lett.* **269**, 441 (1997); *Mol. Phys.* **92**, 723 (1997).

- [15] G. J. Zarragoicoechea, D. Levesque, and J. J. Weis, *Mol. Phys.* **75**, 989 (1992).
- [16] G. J. Zarragoicoechea, D. Levesque, and J. J. Weis, *Mol. Phys.* **78**, 1475 (1993).
- [17] K. Satoh, S. Mita, and S. Kondo, *Chem. Phys. Lett.* **255**, 99 (1996).
- [18] R. Berardi, S. Orlandi, and C. Zannoni, *Chem. Phys. Lett.* **261**, 357 (1996).
- [19] M. Houssa, A. Oualid, and L. F. Rull, *Mol. Phys.* **94**, 439 (1998).
- [20] R. Berardi, S. Orlandi, and C. Zannoni, *Int. J. Mod. Phys. C* **10**, 477 (1999).
- [21] R. Berardi, S. Orlandi, and C. Zannoni, *J. Chem. Soc. Faraday Trans.* **93**, 1493 (1997).
- [22] R. Berardi, S. Orlandi, and C. Zannoni, *Liq. Cryst.* **32**, 1427 (2005).
- [23] R. Berardi, S. Orlandi, and C. Zannoni, *Phys. Chem. Chem. Phys.* **2**, 2933 (2000).
- [24] G. Ayton, D. Q. Wei, and G. N. Patey, *Phys. Rev. E* **55**, 447 (1997).
- [25] G. Ayton and G. N. Patey, *Phys. Rev. Lett.* **76**, 239 (1996).
- [26] T. K. Bose and J. Saha, *Phys. Rev. Lett.* **110**, 265701 (2013).
- [27] D. Guillon, in *Liquid Crystals II*, Structure and Bonding Vol. 95 (Springer, Berlin, 1999), Chap. 5, and references therein.
- [28] D. Miyajima, F. Araoka, H. Takezoe, J. Kim, K. Kato, M. Takata, and T. Aida, *Science* **336**, 209 (2012).
- [29] J. G. Gay and B. J. Berne, *J. Chem. Phys.* **74**, 3316 (1981).
- [30] M. A. Bates and G. R. Luckhurst, *J. Chem. Phys.* **104**, 6696 (1996).
- [31] A. P. J. Emerson, G. R. Luckhurst, and S. G. Whatling, *Mol. Phys.* **82**, 113 (1994).
- [32] D. Adam, P. Schuhmacher, J. Simmerer, L. Häussling, K. Siemensmeyer, K. H. Eitzbachi, H. Ringsdorf, and D. Haarer, *Nature (London)* **371**, 141 (1994).
- [33] M. P. Allen and D. J. Tildesley, *Computer Simulation of Liquids* (Oxford University Press, Oxford, 1989).
- [34] M. Valisko, T. Varga, A. Baczoni, and D. Boda, *Mol. Phys.* **108**, 87 (2010).
- [35] D. V. Matyushov and A. Okhrimovskyy, *J. Chem. Phys.* **122**, 191101 (2005).
- [36] M. P. Allen, *Liq. Cryst.* **8**, 499 (1990).
- [37] See Supplemental Material at <http://link.aps.org/supplemental/10.1103/PhysRevE.89.052509> for a detailed description of the coloration scheme.
- [38] A. T. Gabriel, T. Meyer, and G. Germano, *J. Chem. Theory. Comput.* **4**, 468 (2008).